Accepted Manuscript

Journal of Multiscale Modelling

Article Title:	Fracture Mechanics Assessment of Large Diameter Wind Turbine Bearings
Author(s):	Francois Dagry, Ali Mehmanparast, Patrick Muller, Klaus Pantke
DOI:	10.1142/S1756973718500105
Received:	05 May 2018
Accepted:	11 September 2018
To be cited as:	Francois Dagry *et al.*, Fracture Mechanics Assessment of Large Diameter Wind Turbine Bearings, *Journal of Multiscale Modelling*, doi: 10.1142/S1756973718500105
Link to final version:	https://doi.org/10.1142/S1756973718500105

World Scientific
www.worldscientific.com

Journal of Multiscale Modeling, Volume 10, Issue 4, Article number 1850010
DOI:10.1142/S1756973718500105

Fracture Mechanics Assessment of Large Diameter Wind Turbine Bearings

François Dagry[1], Ali Mehmanparast[2*], Patrick Müller[1] ,Klaus Pantke[1]

[1] Thyssenkrupp Rothe Erde GmbH, Beckumer Strasse 87, 59555 Lippstadt, GERMANY.

[2] Offshore Renewable Energy Centre, Cranfield University, Cranfield, Bedfordshire MK43 0AL, UK.

*Corresponding author: a.mehmanparast@cranfield.ac.uk

Abstract

The structural integrity of large diameter wind turbine bearings have been investigated using the built-in 'contour integral' tool in ABAQUS finite element software package by modelling three-dimensional penny-shaped cracks and evaluating the stress intensity factors. In order to sub-model a crack and investigate the fracture mechanics of the rolling contact between the rollers and the raceway, a python script is developed and implemented in the analysis. Important steps to build the crack model are detailed and recommendations are made for further use of the finite element modelling tool in compressive mixed mode fracture mechanics assessment of wind turbine bearings. Moreover, the influence of initial residual stresses due to induction hardening of the raceway is also investigated and discussed in this paper. For frictionless contacts between the two crack faces, 'contour integral' in ABAQUS appears to be a suitable method to obtain accurate stress intensity factor solutions for mode II and III. The results from this study are validated through comparison with the analytical solutions available in the literature and are expected to facilitate numerical life assessment of wind turbine bearings.

Keywords: Rolling contact, Contact between crack faces, Penny-shaped crack, Subsurface crack, Mixed-mode fracture mechanics, Sub-modelling.

Nomenclature

a	Penny-shaped crack size (radius)
β	Crack angle (with the rolling axis)
θ	Crack tip angle
f_c	Friction coefficient at the crack surface
ν	Poisson's ratio
σ	Stress
P_h	Hertz pressure for the contact
E	Elastic Young's modulus
G	Shear modulus
J	Elastic-Plastic fracture mechanics parameter
K	Stress intensity factor
ΔK	Stress intensity factor range

ε	Strain
FEA	Finite Element Analysis
XFEM	Extended Finite Element Method
SIF	Stress intensity factor
LEFM	Linear Elastic Fracture Mechanics
RS	Residual stress
RCF	Rolling Contact Fatigue

1 Introduction

The continuously increasing demand of clean energy is more and more focused on higher power density outputs from renewable energy sources. In 2016, the installed wind power capacity in the EU reached 153.7 GW [1], and European countries have agreed on a 27% renewable energy target by 2020 [2]. Therefore, wind turbines, which produce electricity from one of the most reliable sources of clean energy: wind, are now constructed with higher rated power capacities and in larger sizes. Hence, the improvement of the integrity assessment of these structures is an essential requirement for the expansion of renewable energy electricity generation from onshore and offshore wind sources.

Wind turbines are comprised of structures such as the foundation, the blades and the slewing bearings which are subjected to complex loading conditions [3]. A breakdown of the five bearings in wind turbine head is demonstrated in Figure 1; one yaw bearing, three for the blades and one bearing for the rotor, which are often subjected to severe loading conditions [4]. The fabrication process employed in preparation of these wind turbine components results in introduction of strain misfit due to thermal expansion, especially during the hardening process. Therefore, residual stresses are induced [5] in the material, which need to be analysed and considered in structural integrity assessments. The main failure mechanism in these bearings is the contact fatigue which occurs between the rolling elements and the raceway [6]. Raceways are typically produced by seamless rolled ring, often made of 42CrMo4 medium carbon steel, and then hardened on the surface to carry the high dynamic wind load [7]. The manufacturing process of large diameter raceways is schematically illustrated in Figure 2, and as shown in this figure, the material is forged, hardened and quenched. Therefore, during the manufacture of raceway, formation of damage in the form of flaws is inevitable. Depending on the size of the inclusions, their position and the flaw density in the material, the raceway is approved or rejected for installation in a wind turbine. These calculations involve fracture mechanics considerations and can assume the inclusion to behave like a crack. By knowing the critical stress intensity factor of the material used for the rings, engineers can perform preventive fracture mechanic assessments.

Inclusions in the raceway of large diameter bearing may lead to a catastrophic failure in case of a fracture mechanics misjudgement. The complex compressive loading state, resulting from the rolling contact, makes a pure analytical analysis approach very difficult. Despite huge progresses made in Finite Element Analysis (FEA) during the last few decades, consideration of mixed-mode fracture mechanics in the presence of residual stresses is still a significant challenge in numerical structural integrity assessment. The current study aims to fill in the knowledge gap by building up a reliable and easy method to assess cracks under complex compressive loading conditions in large diameter bearings by considering the residual stress effects. The present study assumed a penny-shaped crack which is a typical crack shape in life assessment of rolling contact fatigue problems [8]. The results from this

study are validated through comparison with the analytical solutions available in the literature and are expected to improve the life assessment of wind turbine bearings.

2 Stress Intensity Factor Solutions for Penny-Shaped Cracks

In order to characterise the rolling contact fatigue (RCF) behaviour in large diameter bearings used in wind turbines, the linear elastic fracture mechanics (LEFM) theory and the stress intensity factor solutions associated with the penny-shaped crack (see Figure 3), which is commonly employed in rolling contact applications, must be reviewed and understood. For a given crack size and crack angle, the stress intensity factor solution depends on the point considered on the crack tip. Moreover, the stress intensity factor solution depends on the loading conditions e.g. tension or compression and also the fracture mechanics mode.

2.1 Stress Intensity Factors Solutions for Tensile Loading Conditions

The stress intensity factor (SIF) solutions for penny-shaped cracks in an infinite body and under uniaxial tensile loading conditions are derived by Kassir and Sih and Nejati [9], [10] and are summarised in Equation 1, Equation 2, Equation 3 for mode I, II and III, respectively. In these equations, a is radius of the circle crack (i.e. penny shaped-crack size), β is crack orientation, ν is the Poisson's ratio, σ is the applied stress and K_I, K_{II} and K_{III} are mode I, II and III stress intensity factor solutions, respectively. In these equations, the normal stress component on the crack surface $\sigma_{Y_cY_c} = \sigma \cdot cos^2(\beta)$ contributes to mode I fracture mechanics (i.e. crack opening mode) whereas the shear stress component $\tau_{Y_cZ_c} = \frac{\sigma}{2} \cdot sin(2\beta)$ contributes to mode II (shearing mode) and mode III (tearing mode) fracture mechanics.

$$K_I = 2\sqrt{\frac{a}{\pi}} \cdot \sigma \cdot \cos^2(\beta) \quad \text{Equation 1}$$

$$K_{II} = 2\sqrt{\frac{a}{\pi}} \cdot \sigma \cdot \frac{1}{2-\nu} \cdot \sin(2\beta)\cos(\theta) \quad \text{Equation 2}$$

$$K_{III} = 2\sqrt{\frac{a}{\pi}} \cdot \sigma \cdot \frac{(1-\nu)}{2-\nu} \cdot \sin(2\beta)\sin(\theta) \quad \text{Equation 3}$$

2.2 Stress Intensity Factor Solutions for Compressive Loading Conditions

The SIFs for the uniaxial compressive cases are also studied by Kassir, Sih and Nejati [9], [10] and are summarised in Equation 4, Equation 5 and Equation 6 for mode I, II and III, respectively. Note that under a compressive loading condition, the crack is closed, therefore the opening mode (i.e. mode I) does not exist anymore and the SIF for mode I is equal to zero. As for the shear stress component, it takes into account the contact between the two crack faces. Considering the Coulomb law [11] for the friction coefficient f_c, the stress derived from a slipping contact is $\tau c = fc \cdot \sigma_{Y_cY_c}$, with $\sigma_{Y_cY_c} = \sigma \cdot cos^2(\beta)$. The penny-shaped crack SIF for mode II (i.e. shearing mode) and mode III (i.e. tearing mode) are derived from the total shear stress $\tau_{total} = \tau_{Y_cZ_c} - \tau c$, with $\tau_{Y_cZ_c} = \frac{\sigma}{2} \cdot sin(2\beta)$. The analytical equations for the SIFs, which are summarised below, are valid as long as the contact between the crack faces is not locked (i.e. for a locked contact: $|\tau_{Y_cZ_c} - \tau_c| < |fc \cdot \sigma_{Y_cY_c}|$).

$$K_I = 0 \quad \text{Equation 4}$$

$$K_{II} = 2\sqrt{\frac{a}{\pi}} \cdot \sigma \cdot \frac{1}{2-\nu} \cdot \cos(\theta) \cdot [2fc \cdot cos^2(\beta) - \sin(2\beta)] \quad \text{Equation 5}$$

$$K_{III} = 2\sqrt{\frac{a}{\pi}} \cdot \sigma \cdot \frac{(1-\nu)}{2-\nu} \cdot \sin(\theta) \cdot [2fc \cdot cos^2(\beta) - \sin(2\beta)] \quad \text{Equation 6}$$

2.3 Evaluation of Stress Intensity Factors using Numerical Modelling Techniques

The eXtended Finite Element Modelling "XFEM" and "Contour integral" are the common approaches available in ABAQUS finite element modelling software package which is widely used to numerically calculate the stress intensity factor solution for a given geometry using a stationary crack analysis. Both XFEM and contour integral methods use the same principle to compute the elastic-plastic fracture mechanics parameter, *J*, and subsequently work out the SIF value [12]. The difference between these two numerical techniques lies in how the strain field singularity is introduced in the model to simulate a crack.

The "Contour integral" technique is a built-in tool in ABAQUS to compute both *J* and *K* values in static crack analysis. This method is based on a seam crack definition, which requires careful consideration of the mesh size and type used around the crack tip. In this technique the crack front, as well as the crack line and the crack extension direction must be clearly defined. Then, fracture mechanics *J* parameter is calculated using the following equation [13].

$$J = \int_{\Gamma} W - T_i \frac{\partial u_i}{\partial x} ds \qquad \text{Equation 7}$$

where Γ is a contour surrounding the crack tip with its both ends connected to the crack faces, T_i is as the external forces, u_i is the displacements, w is the elastic strain energy and ds is the contour element. Following the computation of *J*, SIFs are calculated using the following equation [10].

$$J = \frac{1-\nu^2}{E}\left({K_I}^2 + {K_{II}}^2\right) + \frac{1}{2G}{K_{III}}^2 \qquad \text{Equation 8}$$

where $\mathrm{G} = \frac{\mathrm{E}}{2(1+\nu)}$ is the shear modulus of the material.

The "extended finite element method" was developed in 1996 to simulate discontinuities and singularities independently of the mesh [14]. This attractive method does not require the mesh to match with the crack tip geometry. As an extension of the classic solution, enrichment functions are added into the displacement calculation nearby discontinuities (e.g. a crack failure) or singularities (e.g. a crack tip) [15] as explained by the equation below.

$$u^h(x) = \sum_{i=1}^{n} N_i(x) \cdot \left[u_i + H(x) \cdot a_i + \sum_{\alpha=1}^{4} F_\alpha(x) \cdot b_{i\alpha}\right] \qquad \text{Equation 9}$$

There is no need to re-mesh the cracked component during a crack growth analysis when XFEM is employed in the analysis. This makes XFEM a cost-effective and efficient numerical simulation approach. In addition to time-saving for performing the simulation, the XFEM approach also saves the time required for re-meshing parts each time that the crack propagates. Since XFEM does not require a particular mesh for the crack tip, the initial crack positioning becomes also a straightforward task and a single mesh configuration can be used for different crack setups. In a static analysis, XFEM can be used in ABAQUS as a built-in tool for crack modelling. Then, numerical SIF outputs can be requested by simply defining a cracked geometry (e.g. a shell circle in the case of the penny-shaped crack) and a crack domain (e.g. the body of the component). But then, there is no difference with the "contour integral" method to compute the *J* value and extract the stress intensity factors. Reliable

XFEM models for calculation of stress intensity factors under a tensile stress field have been previously developed by other researchers as seen in [13], [16], [17] and [18]. However, for the static crack analysis, the contact definition between the crack faces has been made available only since the ABAQUS 2017 version was released. This recent development to include the contact definition as a built-in tool has simplified the employment of the XFEM technique for fracture mechanics analysis under compressive loads.

In this study simulations were firstly performed with both methods, though XFEM encountered issues with the accuracy of K_{III} and the contact between the crack surfaces (the contact issue was fixed in ABAQUS 2017). Therefore, it was decided to use the ABAQUS "contour integral" built-in tool for its capabilities to precisely adjust the mesh around crack.

2.4 Calculation of Stress Intensity Factors in the Presence of Residual Stresses

Both analytical and numerical approaches have been used by researchers to account for the residual stresses effect on the stress intensity factor mode I. The finite element analysis in [19] and the analytical line spring model in [20] show good results for the stress intensity factor mode I under a compressive residual stress field. However, the stress intensity factors under mode II and III have never been investigated in the presence of compressive residual stresses, such as those induced when the material is surface hardened. Weights or Green's functions could be used to analytically compute these complex stress intensity factor solutions. These functions have the advantage to be only dependant on the shape of the crack. When the stress field is not as simple as the uniaxial loading, or when it includes residual stresses, analytical solutions can be computed by integrating the weight functions, multiplied by the stress field, all over the crack surface. Solutions have been worked out for mode I stress intensity factor of the penny-shaped crack, [21], [22], however, no appropriate weight function solution is available in the literature for the penny-shaped crack, for mode II and III fracture mechanics condition.

3 Existing Fracture Mechanics Methods for Rolling Contact Applications

3.1 Analytical and 2D FEA Approach

Earlier attempts have been made by other researchers to calculate the stress intensity factors under rolling contact fatigue conditions [23], [24], [25], [26] and [27]. The analytical-based study of Hearle and Johnson [27] is the work which gathers the most conclusive solutions and information on this topic. Although the considered crack is in two-dimension (2D), the qualitative deductions remain unchanged. Komvopoulos and Cho proposed a 2D plane-strain FEA approach for rolling contact stress intensity factor calculation in [25]. In their proposed approach, the numerical SIFs are calculated using the relationship between the stresses near the crack tip and the *K* fracture mechanics parameter. Their study provides deeper conclusions on the crack mechanism thanks to the simulation of various friction coefficient and crack positions. The main findings from these studies are summarised below:

- Crack propagation mode: Under rolling contact loading conditions, mode II is the dominant fracture mechanics failure mode. Mode I stress intensity factor is either equal to zero or negligible compared to K_{II}, therefore only the shearing mode II is considered. The significance of fracture mechanics mode III is revealed only when 3D numerical studies are conducted.

- Cyclic loading: The rolling contact analysis assumes a cyclic movement of the load. Therefore, the stress intensity factor range ΔK_I, ΔK_{II} and ΔK_{III} can be derived from the difference between minimum and maximum stress intensity factor values for mode I, II and III, respectively. The SIF range should be used in order to assess the fracture mechanics of the raceway subjected to rolling contact fatigue.
- Crack length and depth: These parameters significantly affect the magnitude of the stress intensity factors solutions [27], [25]. Two types of behaviour are noticed: short cracks (the length of the crack is smaller than the depth) and long cracks (the length is at least two times the depth). SIF solutions given in these references show that the SIF is a function of the horizontal crack position and the solutions are symmetric in the case of short cracks. For long cracks, these solutions are not symmetric, and the SIF range ΔK is different between the trailing and leading tip [27]. The SIFs are dependent on the integral of the shear stress over the whole crack surface, and since the crack is long, the shear stress is not considered constant in the crack area. This explains the none-symmetry between the solution curves obtained at the two tip points. The solutions available in the literature show that the trailing tip maximum values are about 30% greater than those at the leading tip of the crack.
- Rolling contact friction: If a rolling contact friction is considered, a tangential force is added to the normal force of the contact. This has the effect of increasing the maximum negative value at the entry of the rolling cycle, but decreases it at the exit. Therefore, it has no influence on the ΔK parameter [27].

3.2 3D FEA approach

Three-dimensional (3D) numerical studies have been previously conducted by other researchers to calculate stress intensity factors under rolling contact fatigue conditions. An example of a study carried for a contact between a railway and a wheel is given in [28], using the displacement correlation method to calculate the stress intensity factor of the elliptical crack embedded in the wheel. The displacement correlation method was also found in a recent independent study [8] to investigate the friction influence on the SIFs, for a penny-shaped crack. The results are very close to the analytical solutions given by Hearle and Johnson [27], and the 2D FEA by Komvopoulos and Cho [25]. In addition, this 3D FEA study brings new information concerning different crack tip points (i.e. different crack tip angle θ, seen in Figure 3), while only the leading and trailing tip can be investigated with a 2D FEA. The SIF solutions for mode III, which are not widely available in the literature, have also been investigated in [28] and [8]. These new considerations do not change the conclusion that shearing mode II remains the dominant mode of failure: mode II SIFs are about 30% higher than the mode III. Moreover, maximum absolute values of the SIFs are reached for the leading ($\theta = 0°$) and trailing ($\theta = 180°$) tips, these points are the same than those studied in 2D analysis. The mains literature findings brought by 3D analysis are gathered and summarised below:

- Crack propagation mode: The study of mode III is made possible by considering a 3D crack. It reveals a dominance of the mode II failure mechanism.
- Crack face friction: The SIF range is clearly reduced when the friction coefficient in between the crack faces is increased. Studies highlight also the existence of different slip

and stick stages between the crack faces, depending on the crack location [8], [25], [27] (3D) and [24], [26] (2D).

- Tip point: The *K* value is dependent on the tip point considered in the analysis. In 2D analysis, only the 'leading' ($\theta = 0°$ in Figure 3, considering a roller moving in the Z axis direction) and 'trailing' ($\theta = 180°$) tip can be investigated. 3D crack models can compute stress intensity factor all along the crack tip, hence it can consider different crack tip angle θ, between 0° and 180°. Nevertheless, trailing and leading tip remain the main crack tip points for consideration in crack propagation behaviour, since these locations correspond to the maximum and minimum SIFs in mode II. Maximum SIFs for mode III are usually reached around the $\theta = 90°$ position.

3.3 3D FEA approach Adopted in the Current Study

The results and solutions available in the existing literature reveal that only parallel cracks have been considered so far in the past studies and a FEA built-in tool has been never used to accurately describe the rolling contact fracture mechanics problem. In this paper, it has been chosen to determine the SIFs using the contour integral tool, developed by ABAQUS. Tilted cracks are considered in the raceway, in addition to the typical parallel crack, to investigate the influence of the β tilting angle on fracture mechanics SIF solutions. The main motivation for running the numerical simulations in the present study is to complete the work already done on the topic using previous approaches. The use of 3D models will also provide data for different crack tip point rather than only the leading and trailing tip and it further assists mode III solutions being investigated. Moreover, the residual stress (RS) effects on the SIF solutions have been investigated in this study. Although residual stresses should only influence the mean SIF values and have no influence on the SIF range, the purpose of this study is to explore the efficiency of a simple numerical tool for complex loading conditions (residual stresses added to the mechanical rolling contact), and for mixed mode fracture mechanics with contact in between the crack faces.

4 Finite Element Modelling of the Rolling Contact Fatigue in Large Diameter Bearings

In the present study, two ABAQUS models have been developed: a rolling contact analysis for large diameter roller bearings, and a coupled penny-shaped crack model. The ABAQUS model developed to simulate the contact between the roller and the raceway is shown in Figure 4. The main parameters of the model are the roller diameter, the roller length, the contact pressure, the roller profile (crowned or logarithmic profiles) and the residual stresses induced into the raceway. For computational efficiency, a quarter of the full geometry is simulated. A Hertz contact pressure $P_h = 1600\ MPa$ is chosen as it is above the fatigue limit of $1500\ MPa$ given in the norm ISO 281 [29]. Finally a frictionless rolling contact is considered. The validity of this model has been investigated through comparison of the obtained FEA results with analytical elastic half space theory solutions [30] and [31], in Figure 5, without considering residual stresses. It can be seen in this figure that accurate results have been obtained from 3D simulations of the rolling contact and the model can be further used for the fracture mechanics analysis.

4.1 Introduction of a Crack using the Sub-Modelling Technique

Due to the gap size between the bearing (e.g. the raceway is about $2\ m$ diameter) and the crack (e.g. $a = 0.2\ mm$), a sub-modelling method has been investigated and used for fracture

mechanics simulations with the rolling contact. There are two different ways to use the sub-modelling method in ABAQUS; using the stress or the strain of the global model to drive the sub-model. As displacements are the most accurate variable in FEA software, the strain results of the rolling contact simulation are used in this work to constrain the sub-model block containing the crack. A boundary condition is created for each exterior surfaces of the sub-model, to allow the global model to drive these faces. After moving the sub-model block to the desired location considering the global model axis system, the software automatically recognises the global nodes and applies the displacements on the driven faces of the smaller model. The range of crack angles simulated is $\beta = -90°$ to $\beta = +90°$, where $\beta = 0°$ represents a parallel crack. Geometric limitations due to the use of sub-models, restrain the study of cracks too close to the boundaries of the raceway. Thus, the crack must lye below a depth of about $0.4\ mm$ (depending on the model).

4.2 Finites Element Model for Fracture Mechanics Study

Only half of the penny-shaped crack is simulated using the X-symmetry boundary condition, as demonstrated in the final geometry and partitions of the crack modelling problem in Figure 6. The crack and its surrounding elements (crack line, crack front and nearby partitions) have to be carefully defined. Two tube partitions are designed along the crack line. The smaller tube will specifically contain the singular elements needed to model a crack and has a radius equal to $0.033 \times a$. The element comprised in the bigger tube will be used for the SIF calculations and its radius is equal to $0.15 \times a$. The crack geometry built is fully proportional to the typical crack size a. Hence, every crack length can be studied in the same way and such cracks will be easy to implement in a python code. Special attention is also carried on the mesh design around the crack line and within the crack front tubes, as the nodes will be used in the *J*-integral calculations. Elements sharing nodes with the crack line must be defined as 'WEDGE' elements. In addition, others element of the crack front must be 'HEX' assigned. These element types are mandatory to request the SIF and *J*-integral field output at the end of the simulation. A suitable proportion for the number of elements within a slice of the crack front was found to be seven elements in the radial direction. Figure 7 shows a typical mesh used around the crack tip, viewed with a cut in the crack plane.

In order to model a crack within the component, the mesh needs to be broken between the two crack surfaces to allow a relative movement of the crack faces' nodes. ABAQUS will duplicate the nodes lying on this crack surface. Sharp cracks are complex to deal with, as they introduce singularity within the strain field. To ensure linear elastic fracture mechanics criteria is satisfied in the analysis, singularity has been assigned at the crack tip by choosing appropriate options in the software (single node for the collapsed element side, and 'midside node parameter' equal to 0.25, [12]). For the study of the embedded penny crack, q-vectors are specified as shown in Figure 7 to define the crack extension direction collinear to the radial direction of the circle. Coordinates of the q-vectors, written in the (X, Y_c, Z_c) axis system follow the $(sin\theta, 0, cos\theta)$ format. After examining different distribution pattern for the q-vectors along the crack front, nineteen q-vectors were found to be a good proportion to mesh the cracked components in this study. Therefore, a ten-degree angle separates two successive q-vectors. Note that in ABAQUS, to enable the modification of every q-vector, the user must create an orphan mesh by importing the input file of the model. Finally, height contours were defined at the surrounding crack tip region to ensure convergence and accuracy in numerical contour values. In order to ensure the validity of the model and the accuracy of the results, the developed model was subjected to a mesh sensitivity analysis and the optimum global mesh size was found to be 0.05 mm.

4.3 The Contact between Crack Faces

Under compressive loading conditions, the crack will be closed and the faces will be in contact. To simulate this behaviour through finite element modelling, a contact definition between the crack faces is required to prevent from overlapping each other. In ABAQUS, a contact requires a contact property setting, with both normal and tangential behaviour. The tangential behaviour includes the friction definition of the contact. In the normal behaviour tab, the user can choose between different algorithms. The convergence of the numerical calculations as well as the interactions between nodes of the contact pair are affected by the previous settings. In the present work, a 'hard contact' is used with the default algorithm. Then a contact property is assigned to the previous contact interaction, whereas both the 'master' and 'slave' surfaces are specified. The node-to-surface method is chosen, as well as the small sliding formulation. This configuration makes possible an automatic recognition of the common nodes between the two faces, i.e. the crack tip nodes. Therefore, no constraint is formed for these nodes and the simulation can run without a fatal error.

4.4 Introduction of Residual Stresses

There are different techniques available to introduce residual stresses in finite element models. In the present work, 'predefined stress field' is used to assign a stress tensor to the desired cells. The compatibility of the SIF calculation and the use of this initial stress field is discussed by Yuebao Lei in [32]. The induction hardened raceway is discretised into several finite cells which slice the depth of the component; a stress tensor is then applied to the cells. The values of the stress tensor components are based on neutron diffraction residual stress measurements which vary through the depth of the raceway. The residual stress profile obtained is displayed in Figure 8. Studies which have used different measurements methods, present the results for residual stresses in induction hardened steel [33], [5]. The profiles and numerical values are similar to what is obtained for large diameter raceways [34], and therefore, can be used instead. Deeper details on the high strength low-allow steel 42CrMo4 typically used in large diameter bearings are presented in [7]. This study provides different hardness and strength data for the three different layers (case, transition layer and core) resulting from the induction hardening process.

4.5 Python Coded Model

In order to speed up the simulation process, a python script has been coded, taking into account the configurations required for modelling including creation of the cracked geometry, creation of an orphan mesh, defining q-vectors, adding the residual stress state and post-processing the simulation results. The purpose of the python script is to generate similar results for a wide range of crack situations, in a reduced amount of time. Simple analysis like the comparison between analytical solutions and FEA required only one simulation for each crack angle (Figure 9 and Figure 10). However, the rolling contact fatigue analysis could not be possible without a code. It required 21 different models to build Figure 16 in addition to 21 more models for Figure 17 (one simulation to get one point). In Figure 19, a total of 2250 simulations have been run to get the curves. The ABAQUS user guide [35] provides detailed script lines and helpful advices to build such a 'contour integral crack' model. The code developed in this study is directly derived from this guidance.

5 RESULTS AND DISCUSSION

5.1 Comparison of Numerical Predictions with Analytical Solutions for Uniaxial Compressive Loading Conditions

In order to validate the developed finite element model, analytical solutions of the SIFs, obtained from Equation 4, Equation 5 and Equation 6 are compared to ABAQUS simulation results obtained from the 'contour integral' technique. To compare with analytical equations, the finite element crack model must consider an infinite body under uniaxial loading conditions. The chosen crack ($a = 1\ mm$) is embedded in the middle of a $20\ mm$ sized cube. This configuration is considered to be sufficient to satisfy the infinite body assumption.

The stress intensity factor results, for mode II and mode III, obtained from FEA simulations are compared with the analytical solutions and the results are shown in Figure 9 and Figure 10, respectively. The results presented in these two figures were obtained with an applied stress of $\sigma = 100\ MPa$ and a friction coefficient $f_c = 0$. Three crack orientations are worked out: $\beta = 0°, 20°$ and $45°$. Steel material properties are assigned to the body, with a Young's modulus of $E = 210\ GPa$ and Poisson's ratio $\nu = 0.3$ [7]. It can be observed in these two figures that there is a very good agreement between FEA predictions and analytical solutions for K_{II} and K_{III}. As seen in Figure 9, for $0° \leq \theta \leq 180°$, K_{II} remains zero when $\beta = 0°$, though for $\beta = 20°$ and $\beta = 45°$, positive values of K_{II} are obtained for $0° \leq \theta \leq 90°$ with a decreasing profile and largest value at $\theta = 0°$, whilst inversely mirrored trends (with respect to the horizontal axis) with negative K_{II} values are obtained for $90° \leq \theta \leq 180°$. The results for K_{III} values in Figure 10 show that similar to mode II, mode III SIF values remain zero for $0° \leq \theta \leq 180°$ when $\beta = 0°$, whilst symmetric trends (with respect to the vertical line at $\theta = 90°$) with an increasing profile and largest value at $\theta = 90°$ are obtained for $\beta = 20°$ and $\beta = 45°$. Also comparison of Figure 9 and Figure 10 reveals that K_{II} values are positive only for $0° \leq \theta \leq 90°$ whereas K_{III} are always positive for $0° \leq \theta \leq 180°$. In addition, no oscillation is observed for the numerical results and smooth trends are obtained from FEA simulations which are consistent with analytical solutions.

Though not shown here for brevity, further FEA simulations were performed with friction coefficients of $0.1, 0.2\ and\ 0.3$. The error analysis between FEA and analytical solutions for mode II and mode III SIF values has been conducted for these friction coefficients, and the results are summarised in Figure 11. As seen in this figure, for $f_c = 0$, the maximum K_{II} error is 0.46 % while this error increases to 1.29 % for K_{III}. As seen in Figure 11 the error in mode II and III SIF predictions compared to analytical equations exponentially increases to over 400% as the friction coefficient increases to 0.3.

Despite good results for mode II and III SIF, ABAQUS computes wrong negative values for the opening mode I. Considering that the crack is closed under uniaxial compression, the mode I stress intensity factor should be equal to zero for the whole range of β angles. The biggest error is reached when the crack is parallel to the raceway and after discussion with the ABAQUS support service, it is concluded that the software is not able to take into account the stress generated by the contact between the two crack faces. This issue affects only the mode I coefficients, as far as the contact is frictionless, but does also affect the mode II and III when a friction coefficient f_c is introduced, as described in Figure 11 for $\beta = 20°$ (note that the error is dependent on the crack angle and parallel crack is the worst situation). The contour integral tool is an efficient solution to extract K_{II} and K_{III} under a compressive field,

K_I is ignored and frictionless contact is preferred. Therefore, this method is used with f_c of 0 in more complex situations, where analytical equations cannot be easily found.

5.2 Penny-shaped Crack Subjected to an Initial Residual Stress Field

In this part, the python script is developed and used to model a penny-shaped crack subjected to residual stresses without any global applied stresses. A crack size of $a = 0.2\ mm$ is used, the contact is frictionless and several crack angles are examined. The model set-up is shown in Figure 12. The stress field aims to represent a typical residual stress state for a given depth of the induction hardened raceway. Therefore, the initial stress tensor of the whole block containing the crack is:

$T = \begin{pmatrix} \sigma_{XX} & 0 & 0 \\ 0 & 0 & 0 \\ 0 & 0 & \sigma_{ZZ} \end{pmatrix}$ At the subsurface, $\sigma_{XX} = \sigma_{YY}$ are negative (i.e. compressive) stresses.

The stress values taken for the following simulations correspond to the residual stresses within an induction hardened raceway at a $0.6\ mm$ depth ($\sigma_{XX} = \sigma_{YY} = -800$ MPa). The residual stress profile used is given in Figure 8. This study considers a crack at the subsurface, hence the initial horizontal stresses are in the negative (i.e. compressive) zone. For higher depths, the stresses switch from negative to positive and finally reach zero at depths far from the surface. This model requires special boundary conditions to retain the predefined field stress within the block.

The FEA results for K_{II} and K_{III} in the presence of residual stresses, without any global applied stresses, are plotted in Figure 13 and Figure 14, respectively. As seen in Figure 13, symmetric trends with respect to the horizontal axis are observed between positive and negative β angles when mode II SIF results are plotted against the crack tip angle. Moreover, it can be seen in this figure that mode II SIF peak values, which occur at $\theta = 180°$ for negative β angles and $\theta = 0°$ for positive β angles, increase by increasing the β angle. It can be seen in Figure 14 that for negative β angles, mode III SIF values are entirely negative for crack tip angles between $0° \leq \theta \leq 180°$, with the maximum value at $\theta = 90°$. These trends are mirrored when positive β angles were applied in simulations. Also seen in this figure is that the peak magnitude of mode III SIF values increase by increase the β angle.

It can be seen that the behaviour of the curves in Figure 13 and Figure 14 (crack under residual stresses without any global applied stresses) is mirrored in Figure 9 and Figure 10 (crack under uniaxial vertical compression) considering the same β angle sign. Under horizontal compressive residual stresses, vertical tensile stresses are generated at the crack faces, which is the opposite of the studied compressive vertical stresses situation. The accuracy of the value cannot be discussed since no analytical solution for such a case is available. Based on the preliminary analytical comparisons made in the uniaxial compressive case, the results are expected to be accurate for these frictionless simulations.

5.3 Numerical Evaluation of SIFs for a Penny-Shaped Crack under Rolling Contact Fatigue Loading Condition in the Presence of Residual Stresses

A rolling contact fatigue loading analysis involving a crack in the raceway in the presence of residual stresses is performed using the developed Python script. A crack size $a = 0.2\ mm$ and depth $d = 0.6\ mm$ (depth of the maximum von Mises stress, see Figure 5) are used, the contact is frictionless in between the crack faces, the Hertz contact pressure P_h of $1600\ MPa$ is applied on the raceway and several crack angles are examined. This part specially focuses

on three crack tip angles: $\theta = 0°$ for the leading tip, $\theta = 180°$ for the trailing tip and $\theta = 90°$ where K_{III} is maximum. These points are the local minimums or maximums for the SIF curves and the main parameters are summarised in Figure 15.

The FEA results obtained from simulations in the absence and presence of residual stresses are presented in Figure 16 and Figure 17, respectively, for the case of $\beta = 20°$. These two graphs confirm that residual stresses act as a mean parameter in such a way that they change the value of the stress intensity factors K, but not the range $\Delta K = K_{max} - K_{min}$. For the crack angle $\beta = 20°$, a shift of $\pm 150\ MPa.\sqrt{mm}$ along the vertical axis is observed between the curve considering residual stresses, and the situation without residual stresses. However, this shift do not change both the shape of the curve and the calculation of the SIF range ΔK.

In order to investigate the influence of residual stresses on SIF, the difference between the SIF range in the presence (i.e. $\Delta K_{with\ RS}$) and absence ($\Delta K_{no\ RS}$) of residual stresses divided by the SIF range in the absence of residual stresses are calculated for three different angles $\beta = 0°, 20°$ and $45°$, and the results are shown in Figure 18. As seen in this figure, for both mode II and III, the stress intensity factor range is insensitive to the residual stresses, as expected, though the maximum and minimum SIF values are influenced by introducing residual stresses in the model. This figure shows that with a gap lower than 1% for the fracture mode II and lower than 3% for the mode III, the simulations confirm that no changes are expected considering the whole rolling contact fatigue cycle in the presence of horizontal compressive residual stresses. However, more research needs to be conducted in future work to investigate how tensile and compressive residual stress profiles affect the rolling contact fatigue crack growth behaviour by changing the mean stress and load ratio. Moreover, the re-distribution of residual stresses and their subsequent impact on RCF needs to be investigated in future work.

5.4 Crack orientation parameter study

Some researchers have found out that the influence of the crack orientation might be hard to model in RCF problems and they developed complex procedures to mesh and compute the fracture mechanics parameters. The study in [10] provides detailed information on how to build such a model, however the required mesh uses tetrahedral elements, and is not compatible with the computations of the built-in 'contour integral' ABAQUS tool. The use of the sub-model in the present study made possible to mesh with hexahedral elements instead and use the ABAQUS computations without any complex post-processing of the finite element results. In Figure 19, the stress intensity factor range $\Delta K = K_{max} - K_{min}$ at the trailing tip has been studied for six different angles in the range of $\beta = 0°$ to $\beta = 90°$. These results are obtained in the absence of residual stress since the computed stress intensity factor range is expected to remain unchanged in the presence and absence of residual stresses as shown in previous section.

The results in Figure 19 show that no significant gaps are observed between the different β angles. Unfortunately, the developed tool is restrained to the study of short cracks ($a = 0.2\ mm\ here$), due to the use of sub-model and geometric limitations especially for tilted cracks. This might explain why results are similar regardless of the crack angle, and conclusion can be different when long cracks are simulated in the raceway. Therefore, long cracks must be studied in the future work and the influence of β angle needs to be investigated and compared to the short cracks.

6 CONCLUSION

The effectiveness of the built-in 'contour integral' tool in ABAQUS has been assessed considering a penny-shaped crack. For mixed mode fracture mechanics involving a contact in between the crack faces, accurate stress intensity factors can be extracted from the software for mode II and III. Key steps of the method used have been detailed, and the crack model was coded in a python script for ABAQUS CAE. Sub-models are used to introduce cracks in the large diameter bearing and the residual stress state resulting from induction hardening process is added to the mechanical rolling contact stress field. Results were generated for mode II and III fracture mechanics, for several crack orientations and for the whole range of crack tip angles. The following conclusions have been made from this study:

- The contour integral is an efficient tool to provide accurate solutions of K_{II} and K_{III} under a compressive stress field with frictionless contact.
- The use of crack sub-models is recommended, and makes easier the meshing procedure with the hexahedral elements required by the ABAQUS software.
- The residual stress field is enabled through the specification of internal stress tensors, and can be easily added to the mechanical rolling contact load. This configuration allows a safe computation of the fracture mechanics parameters.
- The residual stresses act as a mean parameter in such a way that they change the value of the stress intensity factors K, but not the range $\Delta K = K_{max} - K_{min}$ in a rolling contact analysis.
- The study of the crack orientation parameter shows that no significant gaps are observed between the different angles, in the case of short cracks.

Further research needs to be conducted in future work to investigate the residual stress effects on mean stresses and subsequently rolling contact fatigue behaviour of the material using appropriate tools (such as weight functions) and also prediction the stress intensity factors for longer cracks.

REFERENCES

[1] Wind Europe, "Wind in power 2016 European Statistics," 2016.

[2] Wind Europe, "Wind Energy in Europe: Scenarios for 2030," 2017.

[3] B. Lüneburg, D. Becker, and R. Grzybowski, "Development and certification of rotor main bearings for multi MW wind turbine generators," in *Proceedings of the 1st Bearing World Conference 12-13 April 2016, Hanover/Germany*, 2016.

[4] "The driving force in windenergy," *thyssenkrupp Rothe Erde GmbH*, 2017. [Online].

[5] J. Grum, "Induction Heat Treatment and Tribological Property Modification," *Encyclopedia of Tribology*. pp. 1808–1821, 2013.

[6] P. Sauvage, G. Jacobs, A. Menzel, B. Kiefer, B. Lüneburg, and K. Pantke, "Numerical evaluation of steel cleanliness of large main bearings for multi megawatt wind energy turbines," in *Conference for Wind Power Drives*, 2017, pp. 409–424.

[7] P. Göncza, R. Potočnik, and S. Glode, "Fatigue behaviour of 42CrMo4 steel under contact loading," *Procedia Eng.*, vol. 2, no. 1, pp. 1991–1999, 2010.

[8] J. S. Wen, W. E. Ju, T. K. Han, S. T. Choi, and K. S. Lee, "Finite element analysis of a subsurface penny-shaped crack with crack-face contact and friction under a moving compressive load," *J. Mech. Sci. Technol.*, vol. 26, no. 9, pp. 2719–2726, 2012.

[9] M. K. Kassir and G. C. Sih, "Some three-dimensional inclusion problems in elasticity," *Int. J. Solids Struct.*, vol. 4, no. 2, pp. 225–241, Feb. 1968.

[10] M. Nejati, "Finite element modeling of frictional contact and stress intensity factors in three-dimensional fractured media using unstructured tetrahedral meshes," Imperial College London, 2015.

[11] F. K. Chang, M. Comninou, S. Sheppard, and J. R. Barber, "The Subsurface Crack Under Conditions of Slip and Stick Caused by a Surface Normal Force," *J. Appl. Mech.*, vol. 51, pp. 311–316, 1984.

[12] Abaqus/CAE User's Manual, "11.4.2 Contour integral evaluation," 2011. .

[13] M. Levén and R. Daniel, "Stationary 3D crack analysis with Abaqus XFEM for integrity assessment of subsea equipment," Chalmers University of Technology, 2012.

[14] J. M. Melenk, I. Babuška, and I. Babuska, "The partition of unity finite element method: Basic theory and applications," *Comput. Methods Appl. Mech. Eng.*, vol. 139, no. 1–4, pp. 289–314, 1996.

[15] G. Qian, V. F. González-Albuixech, M. Niffenegger, and E. Giner, "Comparison of KI calculation methods," *Eng. Fract. Mech.*, vol. 156, pp. 52–67, 2016.

[16] E. Giner, N. Sukumar, F. D. Denia, and F. J. Fuenmayor, "Extended finite element method for fretting fatigue crack propagation," *Int. J. Solids Struct.*, vol. 45, no. 22–23, pp. 5675–5687, 2008.

[17] F. X. G. Z. de Oliveira, "Crack Modelling with the eXtended Finite Element Method," Técnico Lisbona, 2013.

[18] L. Gigliotti, "Assessment of the applicability of XFEM in Abaqus for modeling crack growth in rubber," KTH School, 2012.

[19] M. H. Gozin and M. Aghaie-Khafri, "2D and 3D finite element analysis of crack growth under compressive residual stress field," *Int. J. Solids Struct.*, vol. 49, pp. 3316–3322, 2012.

[20] R. D. Cordes and P. E. Joseph, "Crack surface contact of surface and internal cracks in a plate with residual stresses," *Int. J. Fract.*, vol. 66, pp. 1–17, 1994.

[21] G. Glinka, "Development of Weight Functions and Computer Integration Procedures for Calculating Stress Intensity Factors around Cracks Subjected to Complex Stress Fields," Ontario, Canada N0B 2H0, 1996.

[22] X. Wang and G. Glinka, "Determination of approximate point load weight functions for embedded elliptical cracks," *Int. J. Fatigue*, vol. 31, pp. 1816–1827, 2009.

[23] A. A. Walvekar and F. Sadeghi, "Rolling contact fatigue of case carburized steels," *Int. J. Fatigue*, vol. 95, pp. 264–281, 2017.

[24] K. Komvopoulos, "Subsurface crack mechanisms under indentation loading," *Wear*, vol. 199, pp. 9–23, 1996.

[25] K. Komvopoulos and S.-S. Cho, "Finite element analysis of subsurface crack propagation in a half-space due to a moving asperity contact," *Wear*, vol. 209, pp. 57–68, 1997.
[26] H. Xu and K. Komvopoulos, "Fracture mechanics analysis of asperity cracking due to adhesive normal contact," *Int. J. Fract.*, vol. 181, pp. 273–283, 2013.
[27] A. D. Hearle and K. L. Johnson, "Mode II stress intensity factors for a crack parallel to the surface of an elastic half-space subjected to a moving point load," *J. Mech. Phys. Solids*, vol. 33, no. 1, pp. 61–81, 1985.
[28] Y. Liu, L. Liu, and S. Mahadevan, "Analysis of subsurface crack propagation under rolling contact loading in railroad wheels using FEM," *Eng. Fract. Mech.*, vol. 74, pp. 2659–2674, 2007.
[29] ISO 281, "Rolling bearings - Dynamic load ratings and rating life." 2010.
[30] H. Zhang, W. Wang, S. Zhang, and Z. Zhao, "Modeling of elastic finite-length space rolling-sliding contact problem," *Tribol. Int.*, vol. 113, pp. 224–237, 2017.
[31] B. Daniel, "Hoch belastete Großwälzlagerungen in Windenergiean-lagen," 2012.
[32] Y. Lei, "Validation of contour integral functions (J and C(t)) in ABAQUS v6.11-v6.14 for combined mechanical and residual stresses," *Procedia Struct. Integr.*, vol. 2, pp. 2566–2574, 2016.
[33] D. Coupard, T. Palin-luc, P. Bristiel, V. Ji, and C. Dumas, "Residual stresses in surface induction hardening of steels: Comparison between experiment and simulation," *Mater. Sci. Eng. A*, vol. A 487, pp. 328–339, 2008.
[34] M. B. Prime, V. Prantil, S. Livermore, F. P. Garcia, and P. Rangaswamy, "Residual Stress Measurement and Prediction in a Hardened Steel Ring," *Mater. Sci. Forum*, vol. 347–349, pp. 223–228, 2000.
[35] Abaqus/CAE User's Manual, "Contour integrals for a conical crack in a linear elastic infinite half space," 2011. [Online].

7 Figures

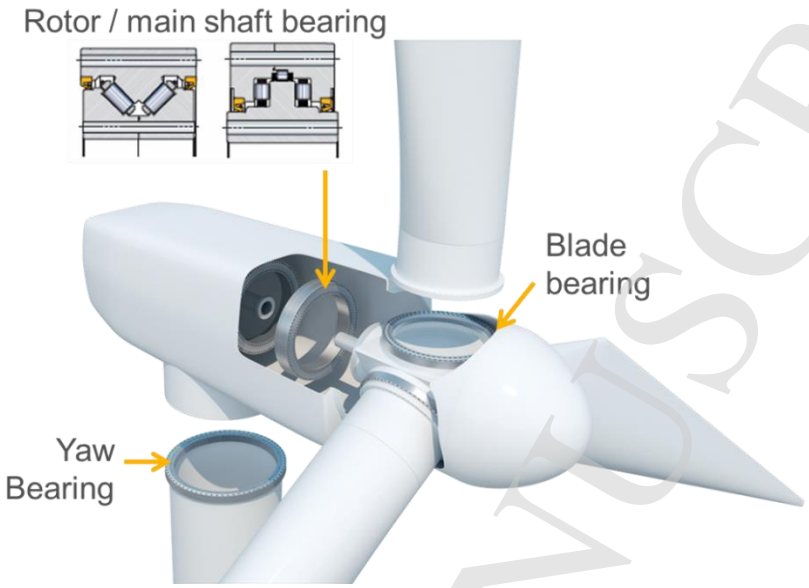

Figure 1: Slewing bearings for wind turbines

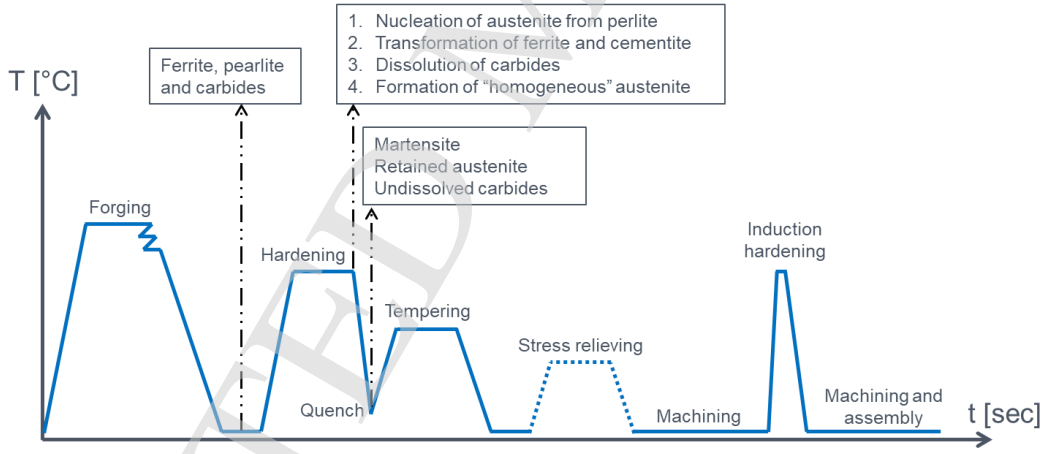

Figure 2: Manufacturing process of large diameter raceways

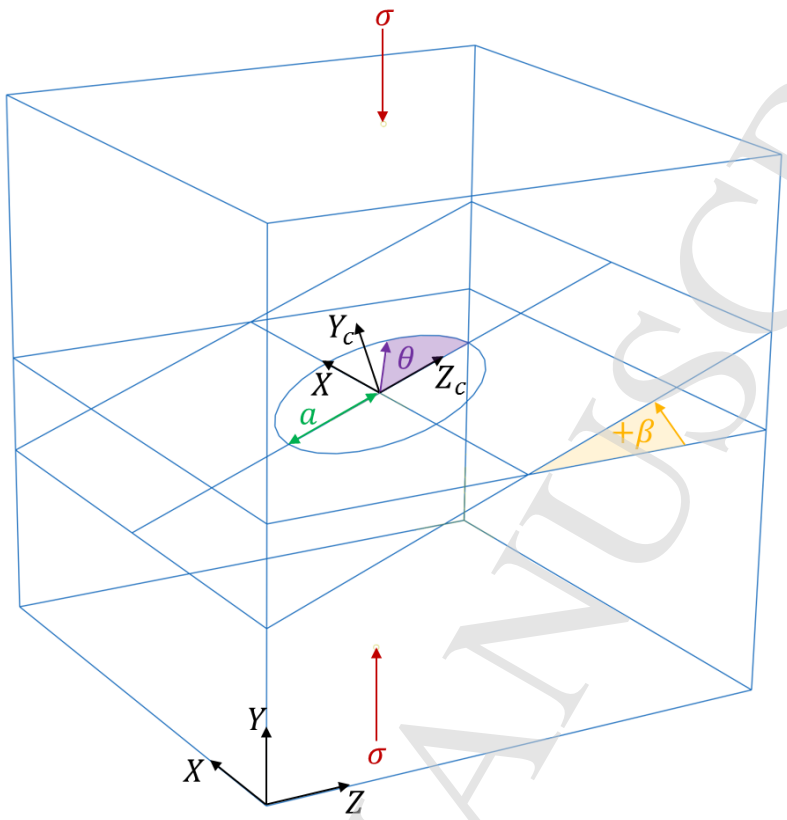

Figure 3: Geometry of the penny-shaped crack under uniaxial compression

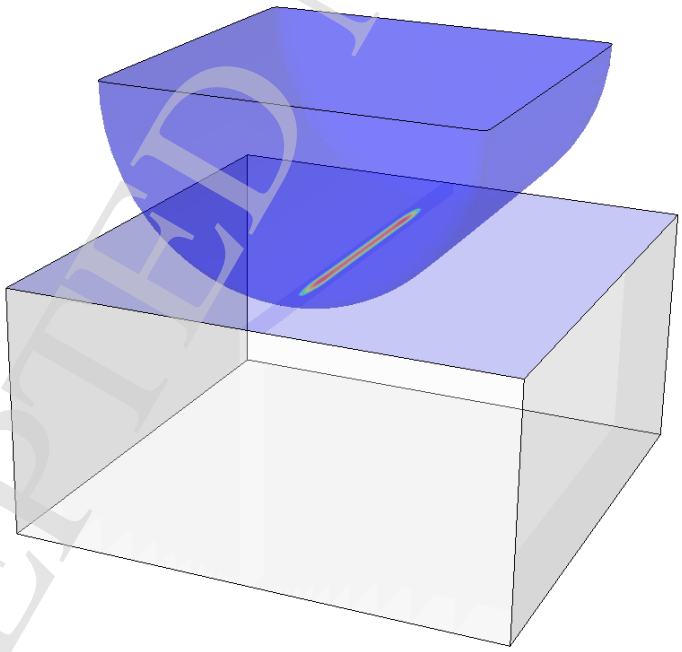

Figure 4: ABAQUS rolling contact model (full geometry)

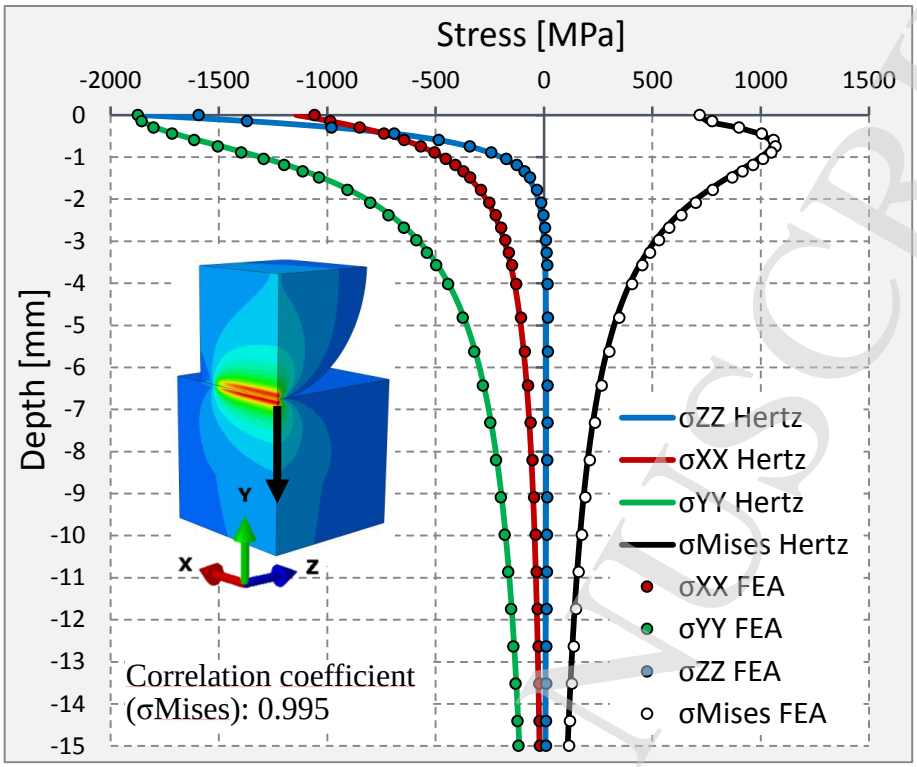

Figure 5: FEA validation with elastic half space theory
$P_h = 1600\ MPa$, without residual stresses and frictionless rolling contact

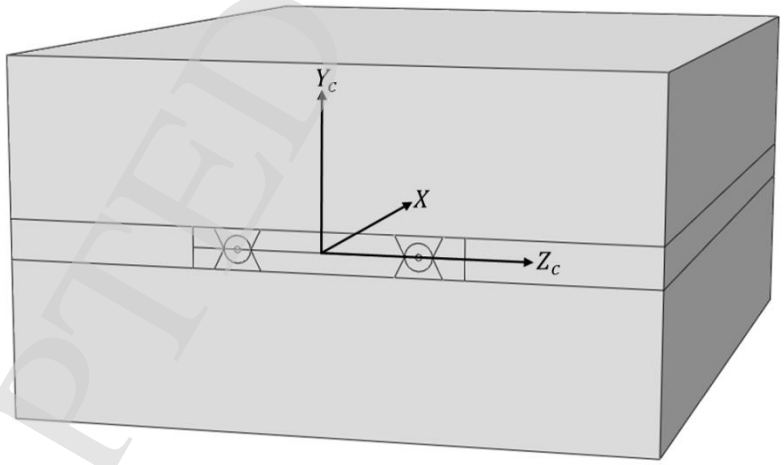

Figure 6: Studied component and created partitions for crack analysis

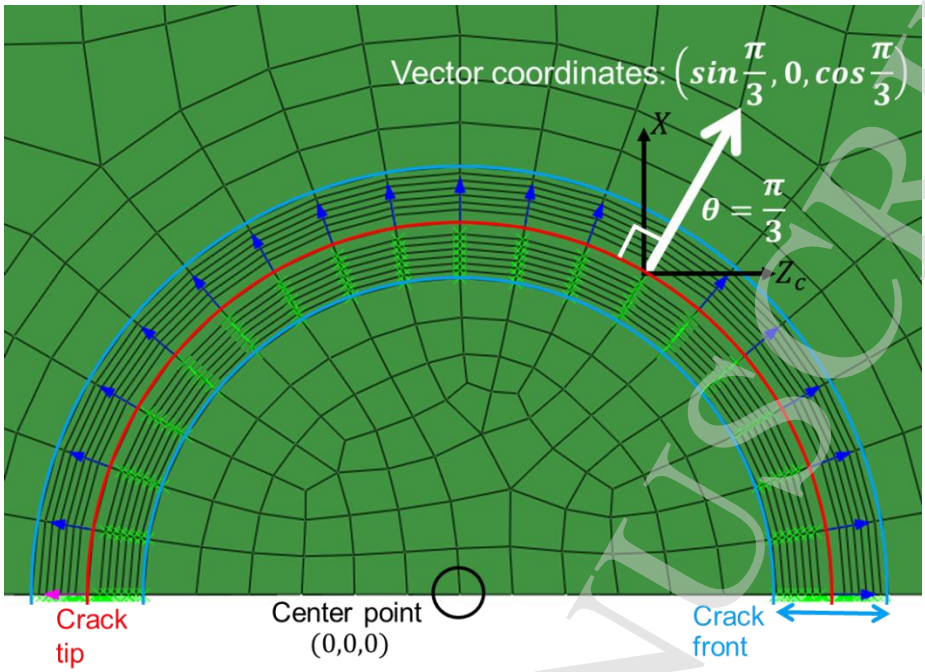

Figure 7: q-vectors set up

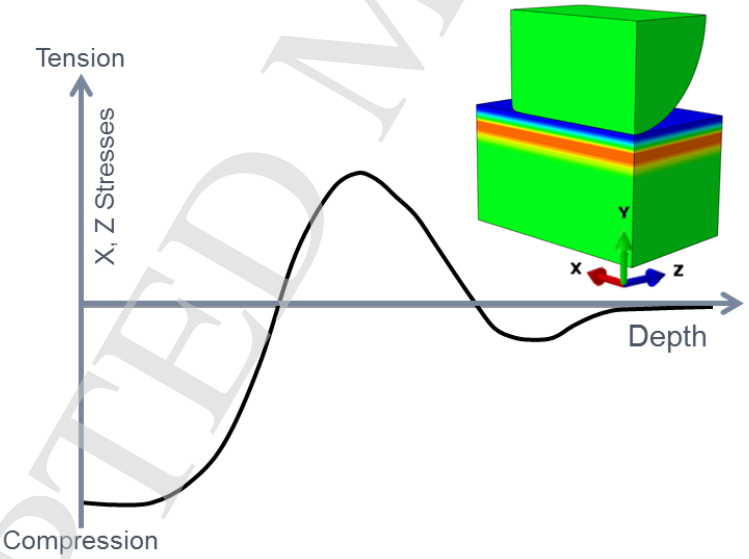

Figure 8: Residual stress profile in a large diameter and induction hardened raceways

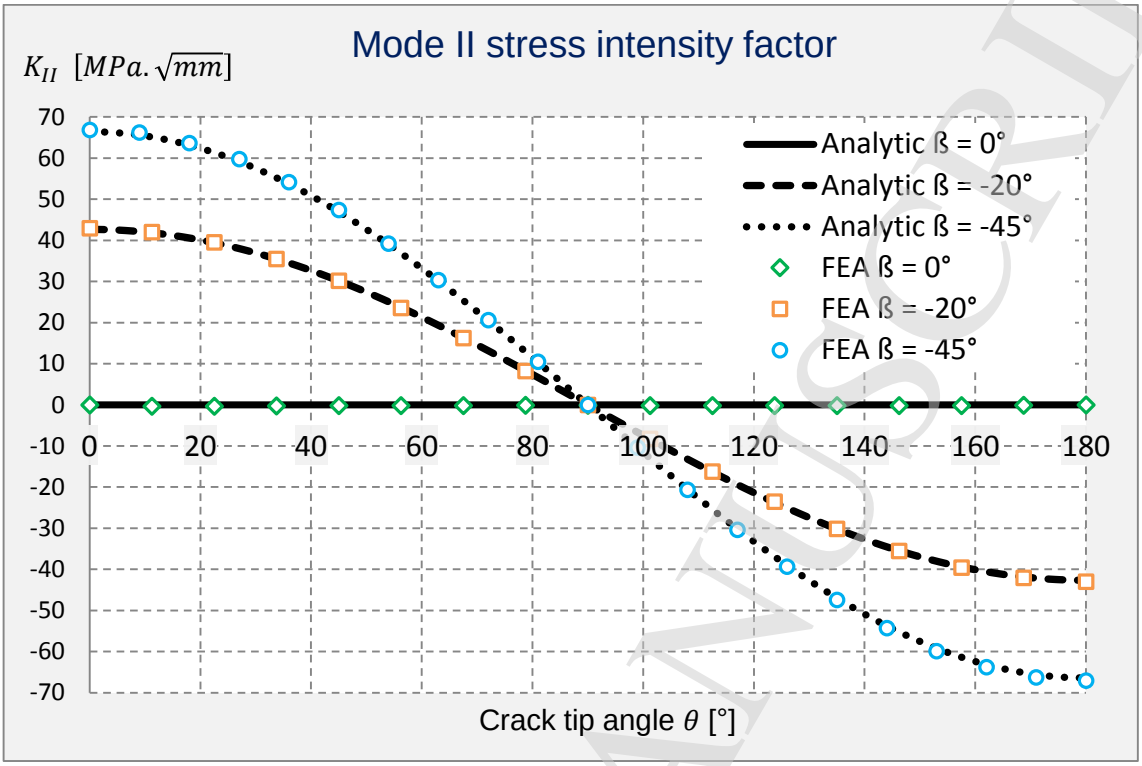

Figure 9: SIF mode II results: comparison between FEA and analytical solutions $a = 1\ mm,\ \sigma = 100\ MPa$, frictionless crack face contact

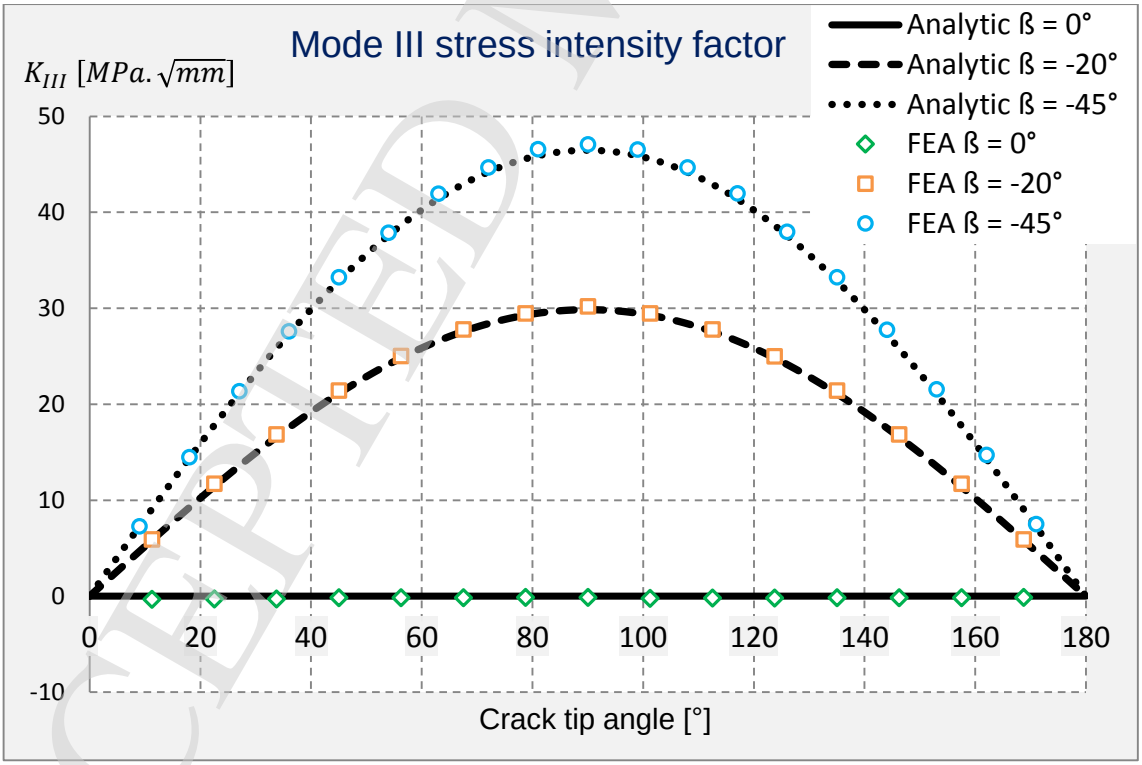

Figure 10: SIF mode III results: comparison between FEA and analytical solutions $a = 1\ mm,\ \sigma = 100\ MPa$, frictionless crack face contact

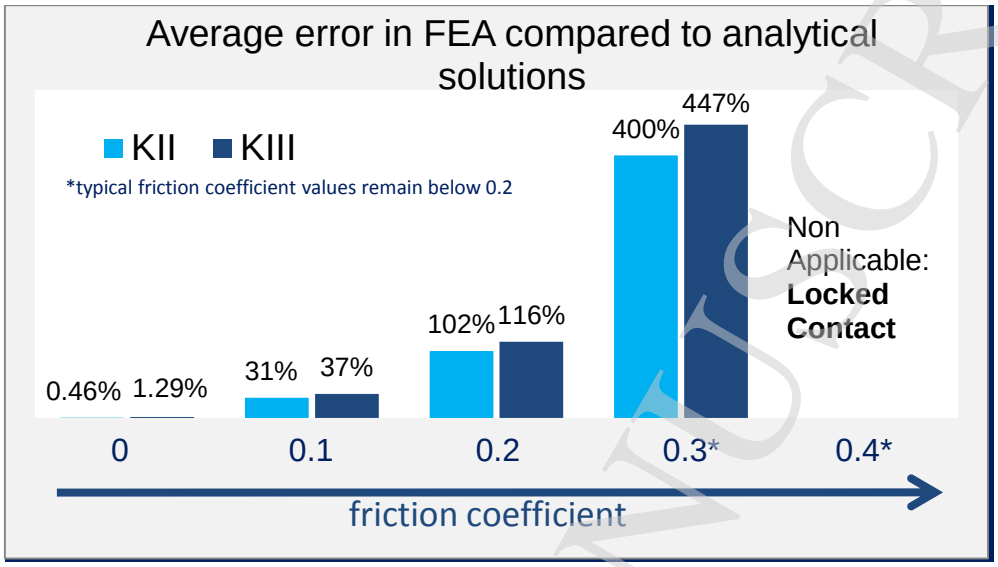

Figure 11: Mode II and III error analysis when the friction coefficient is increased $a = 1\ mm,\ \sigma = 100\ MPa,\ \beta = -20°$

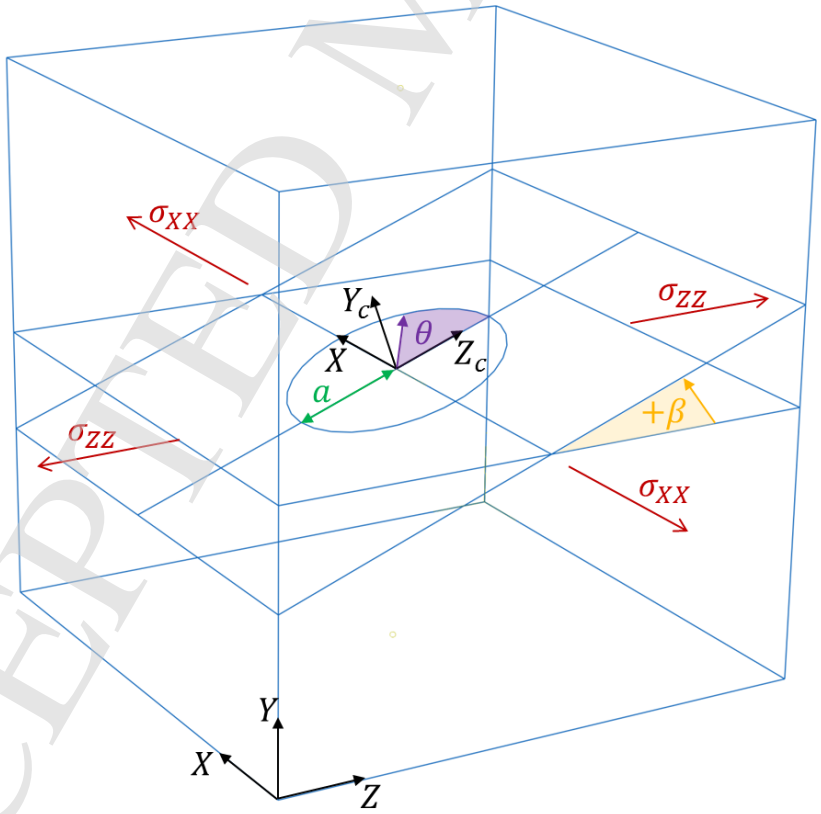

Figure 12: FEA parameters, penny-shaped crack purely under residual stresses without any global stress

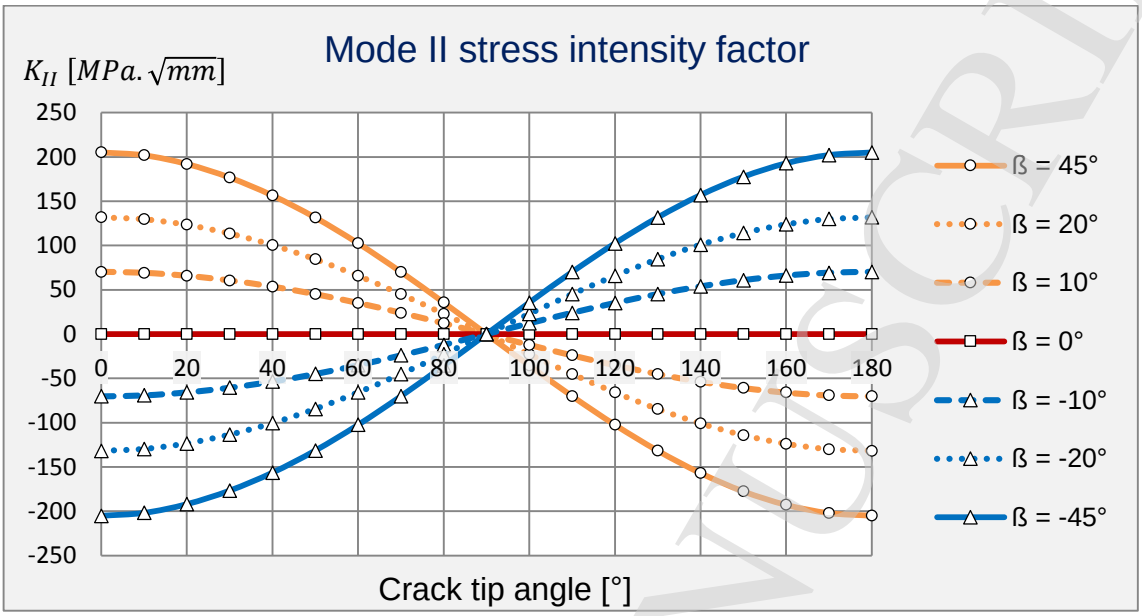

Figure 13: SIF mode II considering residual stresses only
$a = 0.2\ mm,\ \sigma_{XX} = \sigma_{YY} = -800\ MPa$, frictionless crack face contact

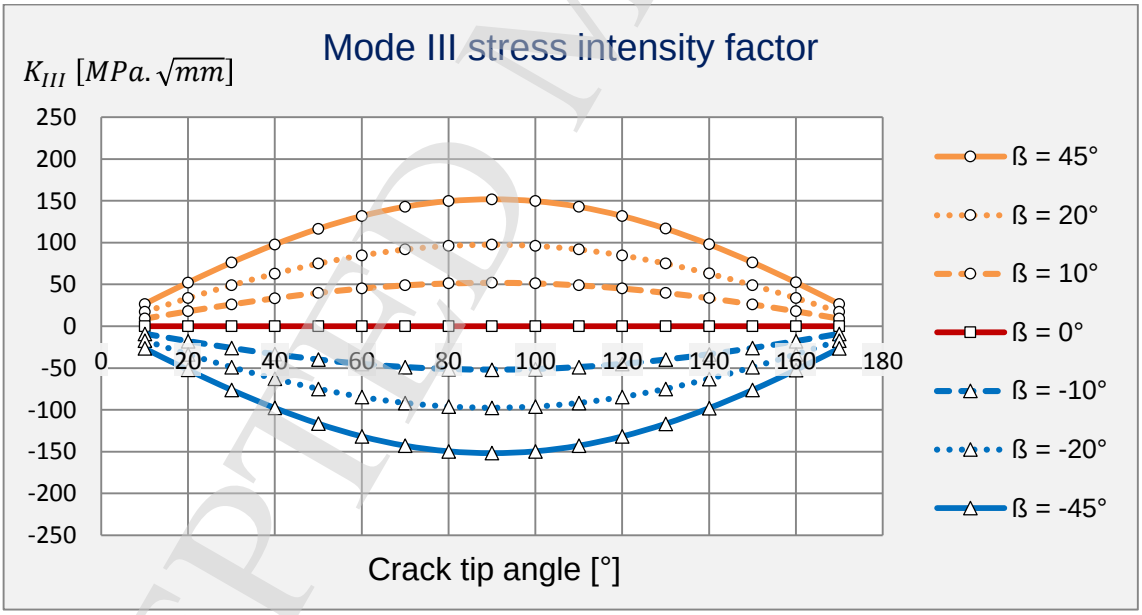

Figure 14: SIF mode III considering residual stresses only
$a = 0.2\ mm,\ \sigma_{XX} = \sigma_{YY} = -800\ MPa$, frictionless crack face contact

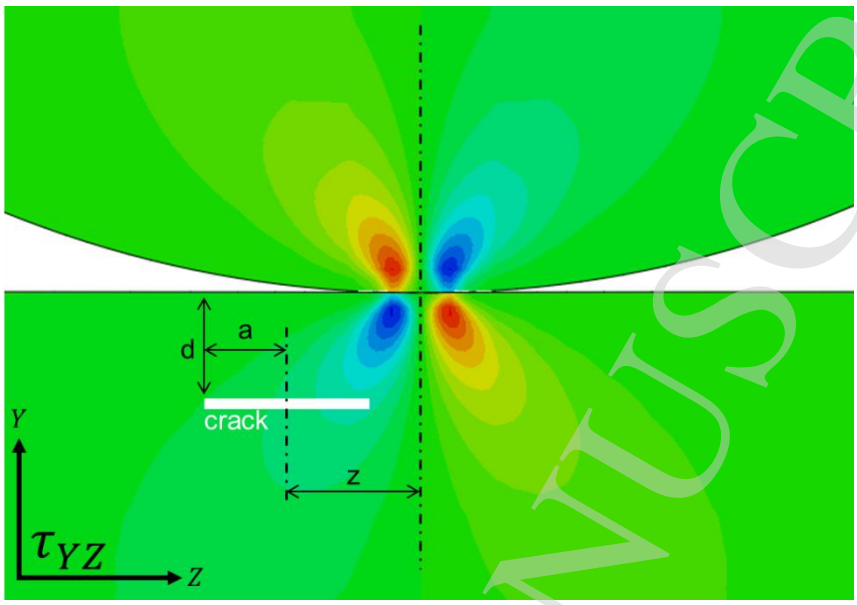

Figure 15: Parameters for rolling contact analysis

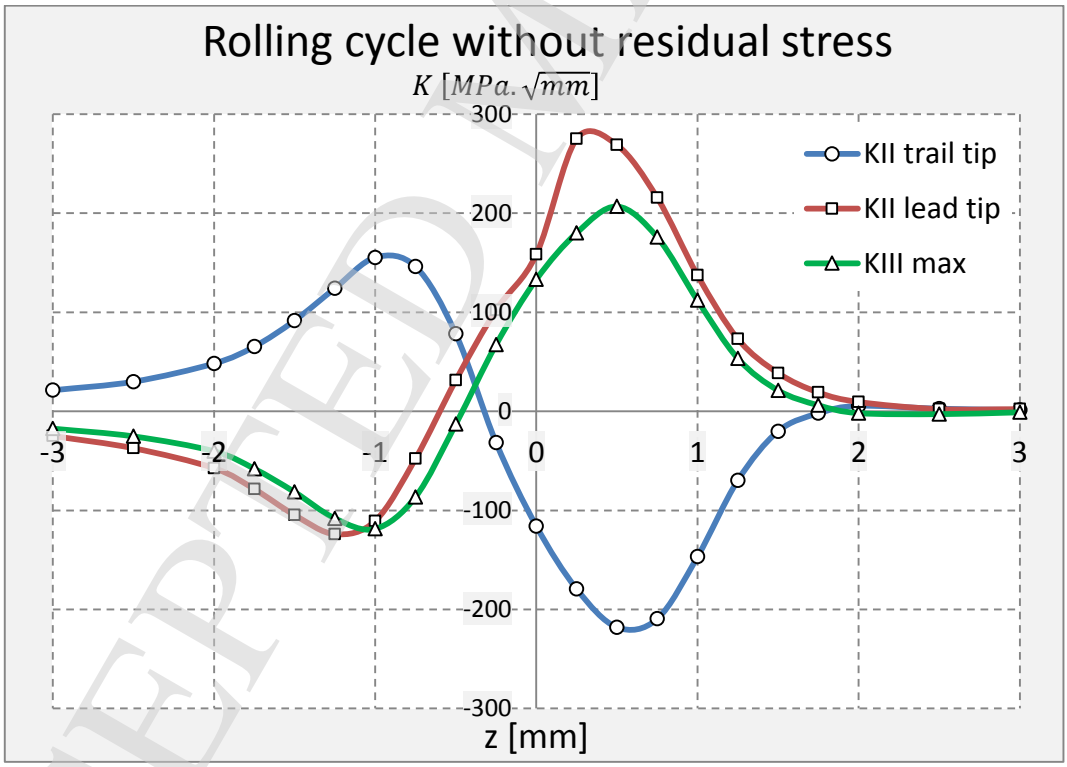

Figure 16: SIF solutions without residual stress, $\beta = -20°,\ d = 0.6\ mm,\ a = 0.2\ mm,$ $P_h = 1600\ MPa$

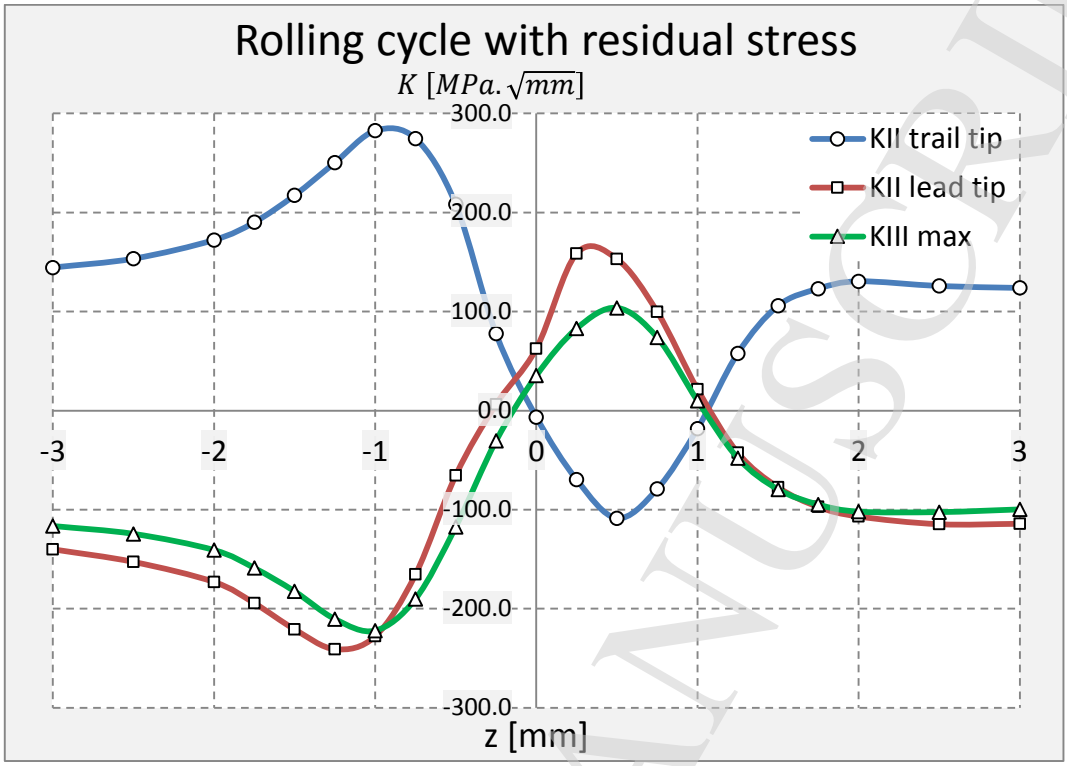

Figure 17: SIF solutions with residual stress $\sigma_{XX} = \sigma_{YY} = -800\ MPa,\ \beta = -20°,\ d = 0.6\ mm,\ a = 0.2\ mm,\ P_h = 1600\ MPa$

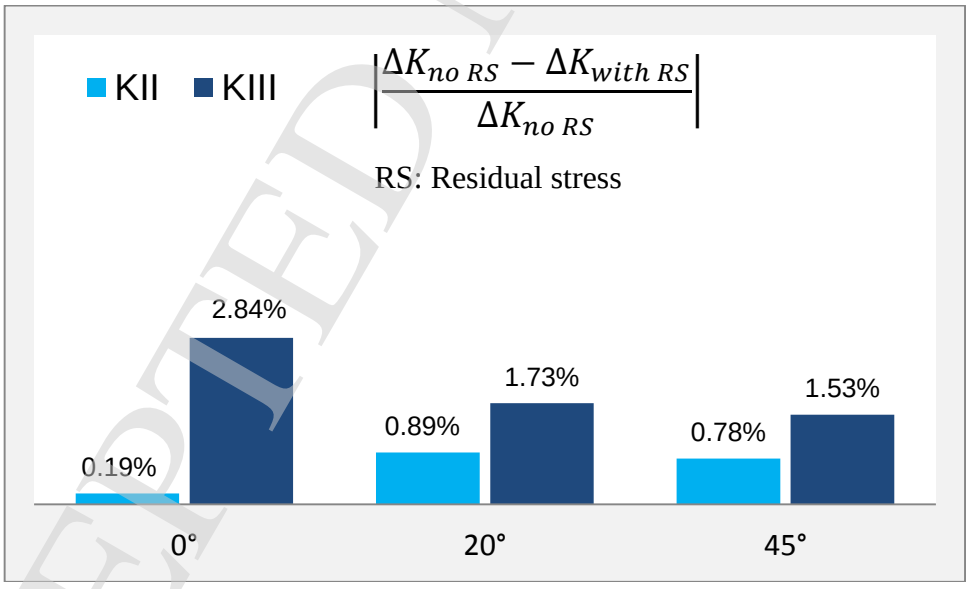

Figure 18: Influence of residual stress on the rolling fatigue SIF

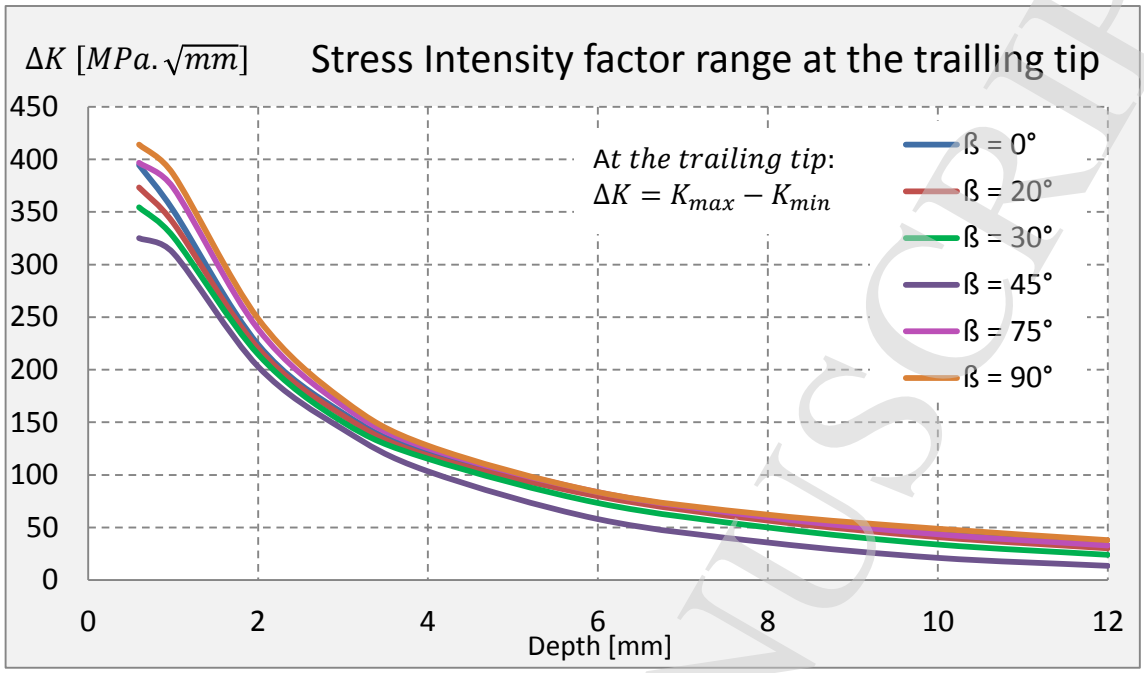

Figure 19: Trailing tip SIF range comparison between several crack orientations $a = 0.2\ mm, P_h = 1600\ MPa$